Spaceborne Scatterometer in Studies of Atmospheric and oceanic Phenomena from Synoptic to Interannual Time Scales

W. Timothy Liu and Wenqing Tang
Jet Propulsion Laboratory 300-323
California Institute of Technology
Pasadena, CA 91109, U.S.A.

1. Introduction

Wind is driven by the differential heating of the atmosphere. Atmospheric water and latent heat are advected by wind. Wind also drives ocean current and transport the heat stored in the ocean. By redistributing the heat in both atmosphere and ocean, wind plays a crucial role in moderating the world's climate. Without wind, the Earth would be a hostile and less suitable habitat.

The ocean and the atmosphere are turbulent fluids with non-linear interaction; processes at one scale affect processes at other scales. Spaceborne sensor is the only potential mean of measuring ocean surface wind forcing at adequate temporal and spatial scales. The microwave scatterometer is designed to measure ocean surface wind. Because microwave penetrates clouds, the scatterometer measures wind under both clear and cloudy conditions. While a passive sensor (radiometer) can measure wind speed, an active sensor (scatterometer) measures both speed and direction. A summary of the principles of scatterometry is given in Section 2.

The scatterometer is a valuable sensor to study meso-s.tale systems, like marine storm, because of its high spatial resolution. Its synoptic and large-scale coverage will help in the monitoring of monsoon and Ekman current (wind driven ocean surface circulation). The repeated global coverage makes it possible to unravel interannual climate signal, such as the El Niño Southern Oscillation. Examples of application of scatterometer observations in studying these atmospheric and oceanic phenomena are given in Section 3-6.

A state-of-ml instrument, the NASA Scatterometer (NSCAT), will be launched in August 1996 and its specifications are described in Section 7. The potential of synergistic application of NSCAT data with other spacebased observations is summarized in Section 8.

2. Scatterometry

A few decades ago, marine radar operators encountered noise on their radar screens which obscured small boats and low-flying aircraft. They termed the noise "sea clutter". This clutter was the backscatter (reflection) of the radar pulses from the ocean surface by the rippling waves on the ocean's surface. The idea of remote sensing of ocean surface winds was based on the belief that these surface ripples are in equilibrium with the local winds. In the last two decades, empirical relations have been developed between the radar backscatter and surface wind based on Seasat [Wentz et al., 19S4] and ERS-1 [Freilich and Dunbar, 1993] data. The principles of scatterometry have be-en discussed by Stewart [1985], Fu et al. [1990], and others.

Spaceborne scatterometers send microwave pukes to the ocean surface and measure the backscattered power. While significant progress has been made in the past two decades on formulating the theoretical link between wind and sea surface roughness [e.g., Plant, 1986; Donelan and Pierson, 1987], large inconsistency between models and observations

remained. The retrieval of surface wind vectors from observations by spaceborne scatterometer relies on empirical relations called "geophysical model function". The model function essentially expresses the normalized backscatter (σ_o) observed by the scatterometer as a function of the equivalent wind speed at a reference level, the azimuth angle between the incident radiation and wind vector (χ), the incidence angle measured in the vertical plane (θ), the frequency of the transmitted microwave, the polarization of the microwave, and a number of secondary non-wind factors, such as sea surface temperature, residual effect of atmospheric stratification, and long waves. For $20°<\theta<65°$, backscattered radiation is believed to be largely resulted from resonant Bragg scattering from short ocean waves, but the effect of non-Bragg scattering from longer ocean waves may also be important. At these, incident angles, σ_o varies approximately as cos (2χ) with maxima at upwind and downwind and minima near crosswind. Since wind shear in the atmosphere depends on density stratification, in addition to surface roughness, the equivalent neutral wind is used with the intention to remove the effect of atmospheric stratification from the model function. A parametrization model of the turbulent transports in the atmospheric surface layer [Liu, et al., 1979] is generally used to relate the real winds to the equivalent winds. The secondary factors on the the relation between wind and backscatter have been studied by Liu [1984], Glazman et al. [1988], and others. The normalized backscatter has also been directly related to the wind-stress at the surface by Liu and Large [1981] and Weissman et al.[1994].

A single measurements of σ_o is insufficient to solve for both wind speed and direction. For the scatterometer on Seasat which has two perpendicularly oriented antennae, up to four solutions are possible even for noise-free measurements [e.g., Long and Mendel, 1991]. The ambiguity in wind direction can be removed, theoretically, by measuring at additional angles, as in the NSCAT design. In practice, however, the model function inversion usually results in multiple solutions having nearly the same speed but differing widely in direction, because of noisy data. While additional processing is still required to select a unique wind direction, the capability of present scatterometers to measure from three azimuth angles reduces the task of selecting the correct wind direction.

3. Tropical Cyclones

Wind observations over ocean are largely made by merchant ships; ship reports are " sparse, particularly within storms. The spatial resolution of numerical analysis at weather center are generally insufficient to reveal accurate position and details. Satellite infrared image may help to locate storms but does not reveal the surface intensity. Spaceborne scatterometers, with the ability to penetrate clouds and measure surface winds at 25-50 km resolution, are useful in the study of synoptic and mesoscale systems over ocean. The potential of scatterometer was first demonstrated in the study of the QE 11 storms by Gyakum [1983] using observations from the Seasat scatterometer when numerical prognoses of major weather centers missed the intensification. Surface pressure which would help to gauge the intensity and to locate the center of the storm can also be derived from scatterometer winds by inverting a boundary model [Brown and Liu, 1982] assuming geostrophic balance. Such application has been demonstrated in mid-latitude storms [Brown and Levy, 1986]. Hsu and Liu [1996] extended such technique to study typhoon (tropical cyclone) by adding a gradient wind balance in deriving pressure field using ERS-1 scatterometer winds.

The detailed structure of the wind-field within the scatterometer ground track in Fig. 1 illustrates the high spatial resolution of the scatterometer. The overlaid of scatterometer winds on precipitable water dramatically visualizes not only the structure of the typhoon, but the relation between the dynamics and the hydrologic balance in the mesoscales. It also

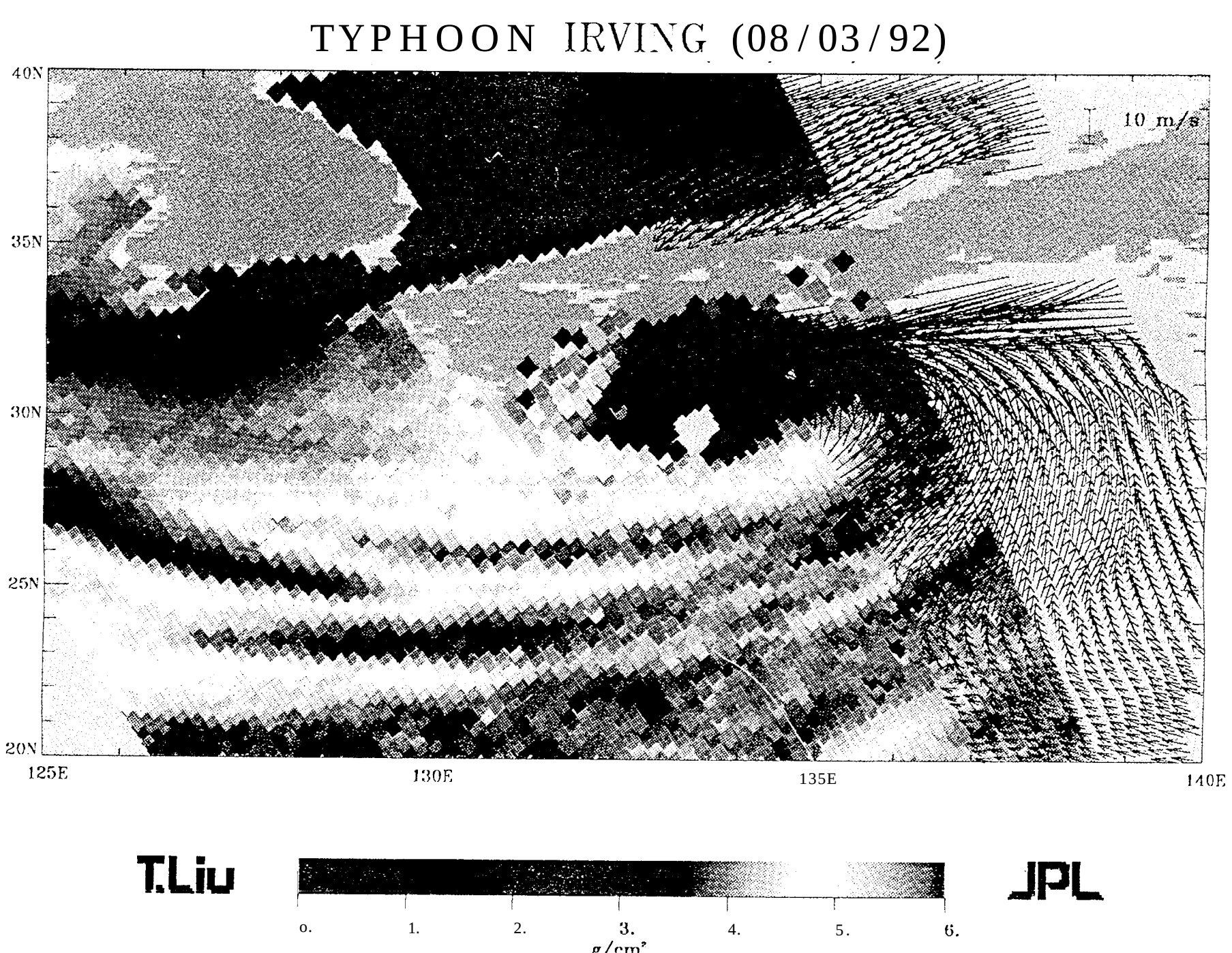

Fig.1 Typhoon Irving revealed by the wind vectors from ERS - 1 scatterometer (dark arrows) and the precipitable warn- from SSMI (color image) as it hits the Honshu Island of Japan on August 3,1992

demonstrates the "all weather" capabilities of microwave sensors. The scatterometer on the European Remote Sensing spacecraft BIN-1 scan onl y on one side of the spacecraft with a swath of 475 km, but other scatterometers have better coverage. The precipitable water was derived from observation of the Special Sensor Microwave Imager (SSMI) which has a much wider swath.

4. Monsoon

Monsoon is the seasonal change of winds which is forced by continent-ocean temperature contrast. Monsoon affects a large area of the world [Ram age, 1971]. It is periodic only in the sense that it comes every year; it has significant intraseasonal and interannual variation [Lau and Li, 1984]. Its annual onset, intensity, and retreat vary greatly, and the variation has strong economic impact and may cause severe human suffering. While the economic impact of the variation is locally felt, the cause of the variation is perhaps seeded in planetary waves, and the effects may be globally felt [Kristnamurti 1985]. Beside. bringing rain to land, monsoon also changes ocean currents and upwelling [e.g., Liu et al. 1992]. Over land the consequences of monsoon are, perhaps, well observed, but the breeding ground over the ocean has been insufficiently monitored. Spaceborne scatterometer with its repeated global observations and unprecedented spatial resolution is conducive to monitoring and understanding monsoon.

The differences between the monsoon in the South China Sea and the Bay of Bengal are obvious in Fig. 2. in the Bay of Bengal, once monsoon starts, the surface wind is strong and steady from June to September, with cross equatorial flow changing from southeast to southwest direction. At the beginning of June, there is a consistent northward surge of water vapor. All the moisture were pushed to the land and coastal area, leaving the atmosphere over the ocean dry. By the. end of September, the humid air returns to the . ocean again. In the South China Sea, however, there are more variabilities; the wind and moisture are oriented in meso-scale weather systems. The same characteristic occurs in subsequent years. The ocean in both regions are warm before monsoon onset, and the temperature is particularly high in the South China Sea. The ocean is cooled in both regions after the monsoon strengthens is summer. In the fall, stronger off-shore winds are found in the South China Sea and the ocean cools further. In the Bay of Bengal, however, wind dies down and the ocean warms up again.

5. Ekman Current

Over small scale and near the equator, the effect of the earth's rotation is small. The relation between wind and current is direct; wind just drags the water along, For example, when a breeze blows over a pond, waves generated follow the wind direction. But over large scale, wind and current is not in the same direction, A century ago, the Norwegian explorer, Nansen, observed that floating ice were moving 20-40° to the right of the wind.

Lagrangian drifters are floats which follow the surface current. After it is deployed, the position of the drifter is tracked by satellite and the current velocity can be computed. The track of the drifters deployed in 1992 are shown in Fig. 3. They follow currents at 15 m depth to within 1 cm/sec [Niiler et al., 1995]. The wind velocity derived from ERS 1 scatterometer were first interpolated to the time and position of the drifter. Then a coherence analysis on the two vector quantities - wind and current, was performed, The phase of the coherence which represents the average angle between the two vectors clearly shows current flows to the right of wind in the Northern Hemisphere and to the left of wind in southern hemisphere. The angle roughly falls between 1 0° to 40°, and should

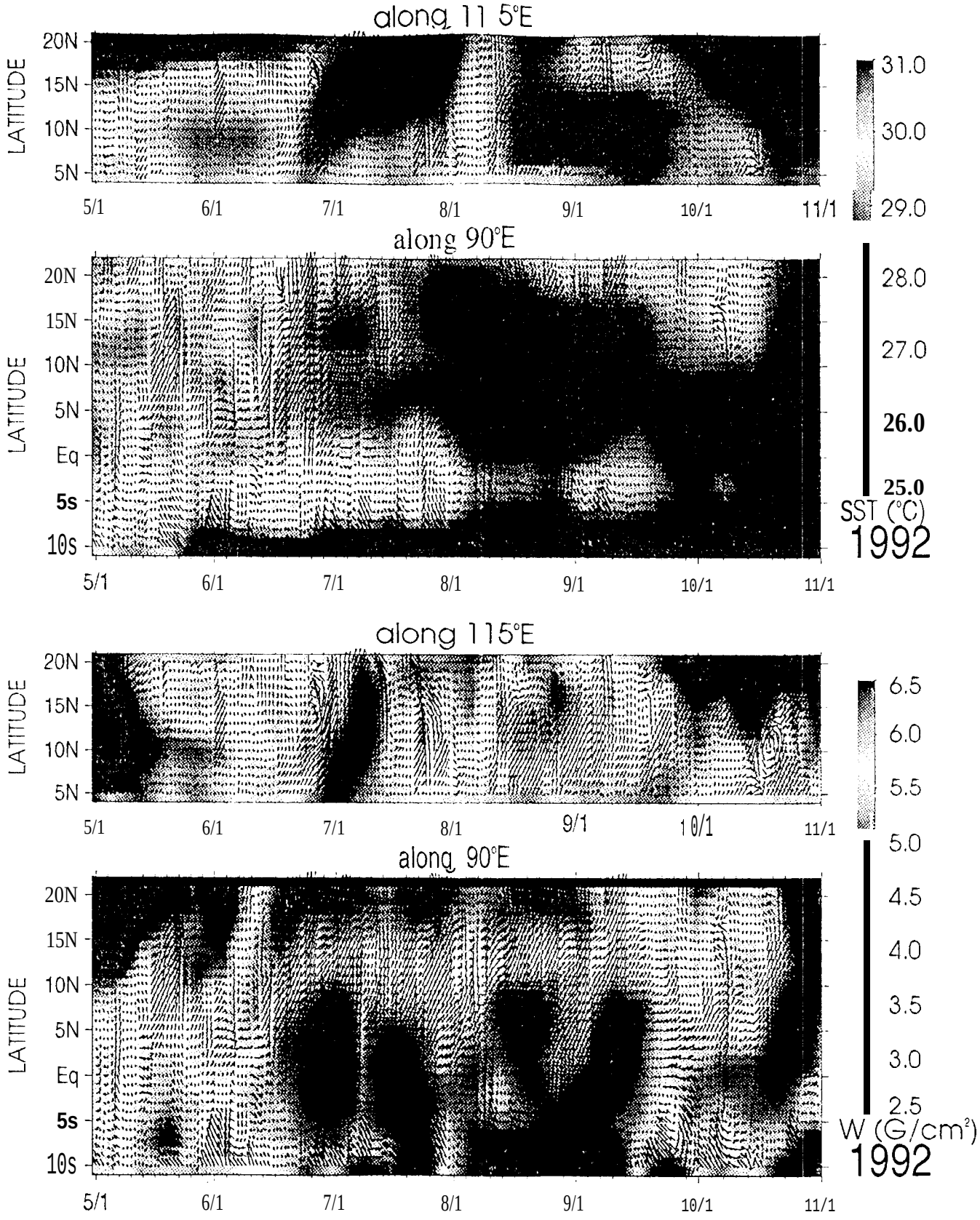

Fig. 2. Latitude-time variations in the South China Sea(115"E) and Bay of Bengal (95°E) of surface wind (black arrows) superposed on the color pictures representing and sea surface temperature (upper) and integrated water vapor (lower), during the monsoon sea son of 1992. The horizontal axis represents time from May 1 to November 1, and the latitudes on the vertical axis run from the north coast of Borneo to the south coast of China at 115°F. and from the South Indian Ocean to the coast of Bangladesh at 95°E. The surface wind field is derived from observations by the microwave scatterometer on ERS- 1, and then interpolated to 10 and seven-day maps through iteration, The sea surface temperature is from AVHRR blended with in situ measurement, and the integrated water vapor is from SS MI.

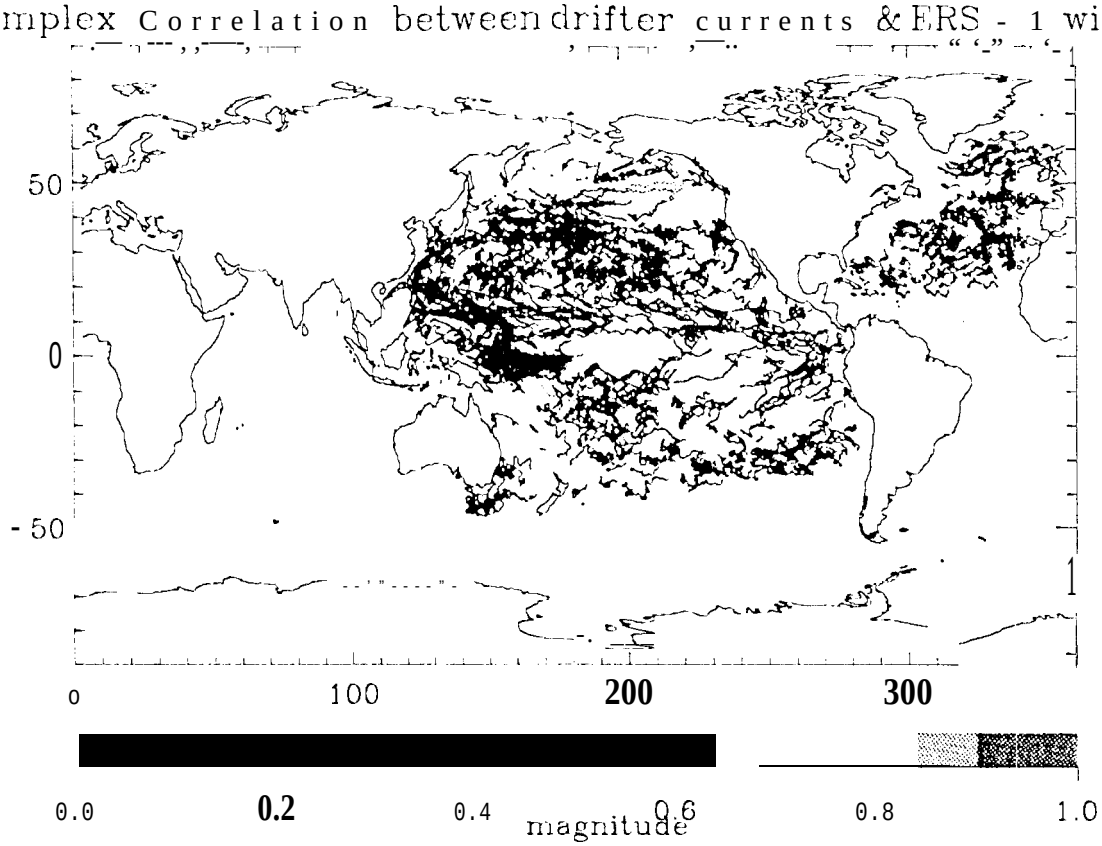

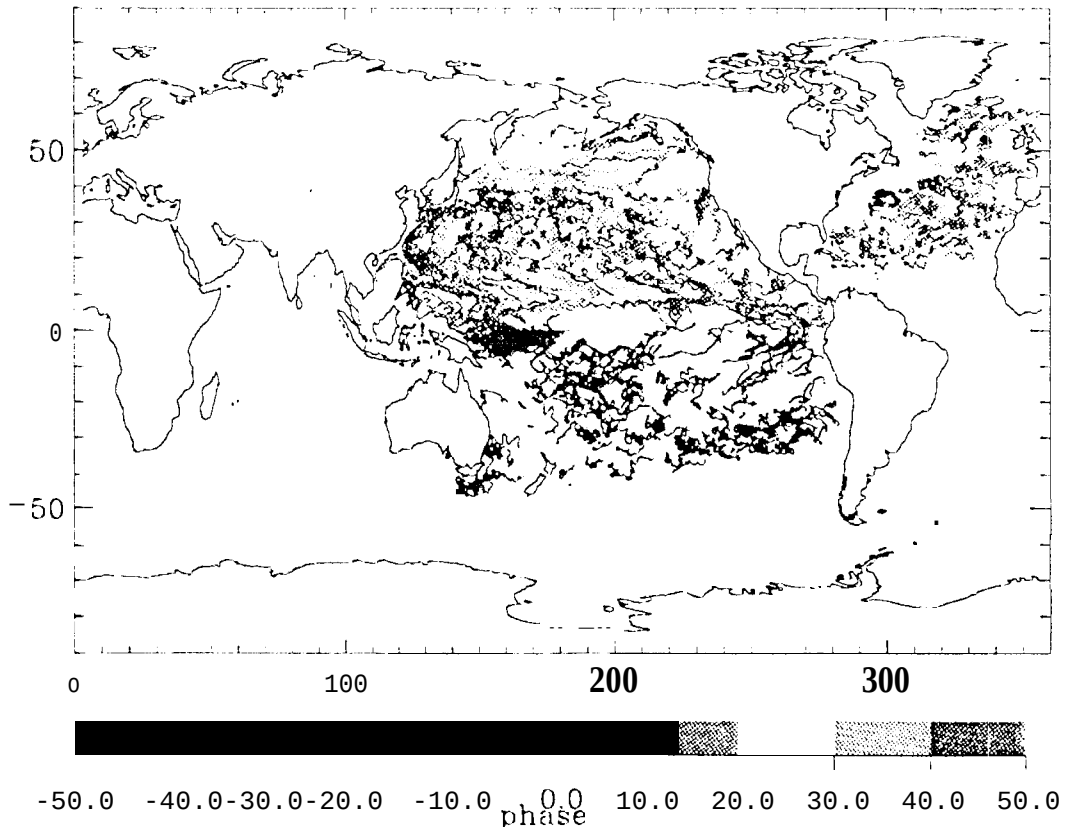

Fig.3. Tracks of Lagrangian drifters deployed in 1992. The colors represent magnitude (upper) and phase (lower) of the coherence. between surface wind velocity derived from ERS-1 scatterometer and ocean current velocity at 15 m depth derived from the drifters. The wind velocity is interpolated to drifter location and time.

varies with latitude (Coriolis force) and depth the mixed layer. The magnitude shows that high correlations are found in the equatorial and mid-latitude oceans where the current is strong and low correlations are found in the subtropical gyres where the current is weak.

The drifter data, in combination of wind forcing derived from the scatterometer and the geostrophic current derived from altimeter data, should be very useful in modeling wind-driven ocean circulation, Such model between surface wind stress and the ageostrophic Ekman velocity (with the geostrophic component removed from the drifter velocity) has been developed by Ralph and Niller [1996] and others.

6. El Niño

On the basis of temporally averaged observations [Rasmussen and Carpenter, 1%2], El Nino has been traditionally viewed as a low-frequency warming of the tropical ocean. Improved observations have revealed that critical intraseasonal phenomena, such as propagation of sea-level variation across the. equatorial Pacific [e.g., Lukas et al., 1984], occur before and during El Nino events. The sea-level changes have been interpreted as the manifestation of equatorial Kelvin waves. These eastward-propagating disturbances in the ocean are confined to a narrow waveguide by the Coriolis force; Kelvin waves have been related to anomalous westerly wind bursts near the date line by theoretical studies and numerical models. The intensity of episodic wind anomalies increases preceding an El Nine) event, as shown by data taken at island stations and at mood buoys [e.g., Luther et al., 1983]. How the synoptic west-wind episodes influence low-frequency changes in surface temperature is still unclear. Documentation on forcing and response is not comprehensive enough to answer this question.

Recently, the evolution of an El Nino warming event in the eastern tropical Pacific at the second half of 1994 was inferred from sea-level rise measured over several months by the microwave altimeter on the Topex/Poseidon spacecraft [Space News, Vol. 6, No. 5, page 13, 1995]. in Fig, 4, four spaceborne sensors were combined to describe this event. The deviations of the 1994 values of a parameter from its corresponding 1993 values are shown and these deviations are, hereafter, referred to as anomalies. In the equatorial eastern Pacific, the Trades Winds generally blow from the west to the east and their zonal components are negative. During the second half of 1994, four distinct groups of equatorial westerly (positive) wind anomalies were observed by the scatterometer on ERS 1 to occur near the date line. Each group of wind anomalies initiated an eastward-propagating, downwelling Kelvin wave that was exhibited as anomalous sea-level rise observed by Topex/Poseidon altimeter. Corresponding to the passage of Kelvin waves are surface-warming episodes observed by AVHRR. Anomalous integrated water vapor observed by SSMI indicate that the westerly wind and warming episodes are also associated with enhanced atmospheric convection.

It is obvious that this anomalous warming event is not continuous, but consists of a series of intraseasonal episodes. Unlike the El Nino events of the 1980s, equatorial warming events in the 1990s are more frequent, last for shorter periods, and are less intense. Whether the 1994 warming can be classified as an El Nino is being debated. The coincident observations infer clearly that the westerly wind anomalies are precursor of El Niño and that spaceborne scatterometer is a valuable sensors in the monitoring, understanding, and prediction of El Niño.

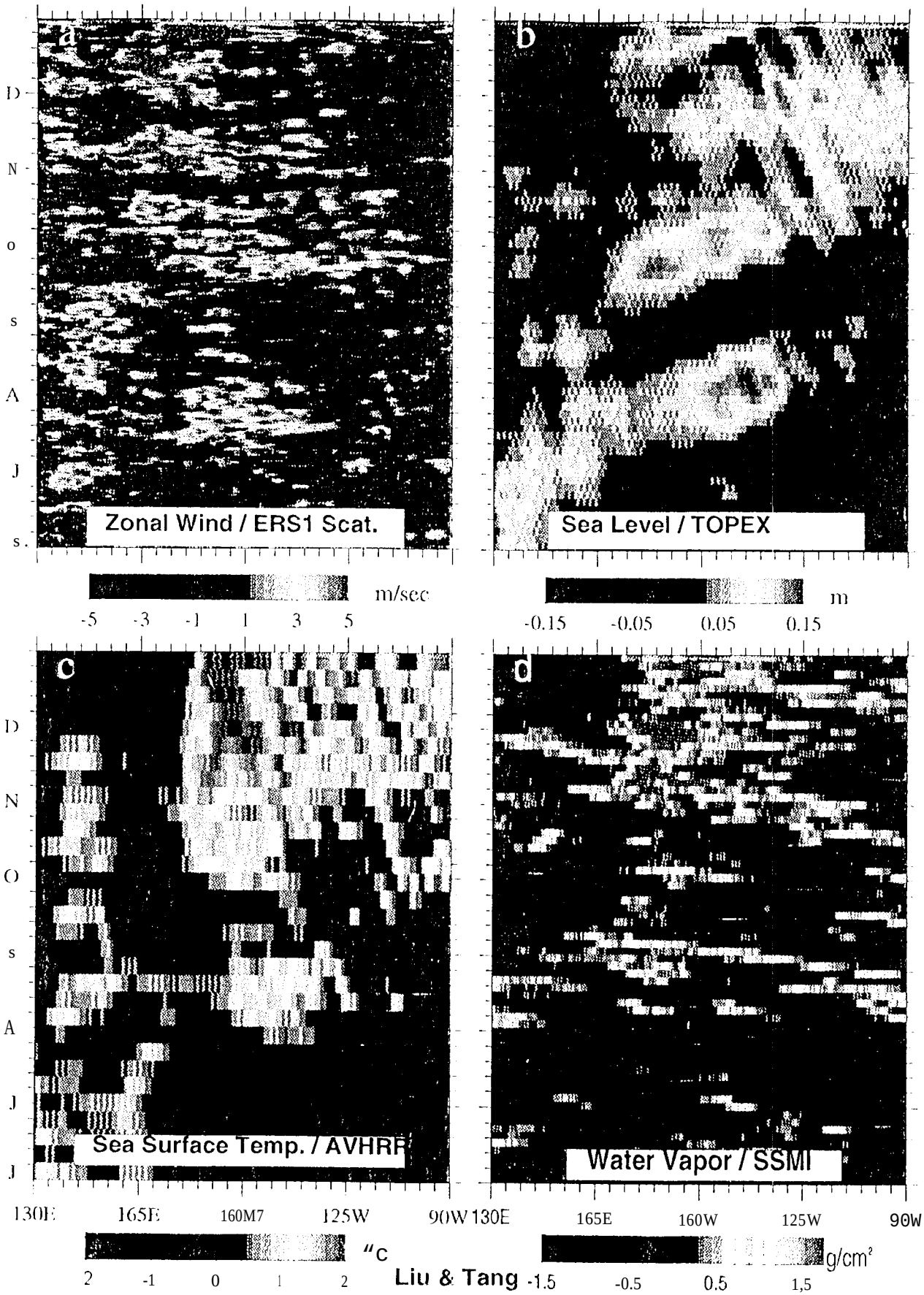

Fig. 4. Time-longitude variations, along the equator, of 1994 - 1993 differences in zonal wind stress derived from ERS-1 scatterometer (upper left); sea level derived from Topex/Poseidon altimeter (upper right); sea surface temperature derived from AVHRR blended with in situ measurements (lower left); integrated water vapor derived from SSM 1 (lower right). The horizont al axis represents longitude from Indonesia across the Pacific to Galapagos. The vertical axis represent time from June to December.

7. NASA Scatterometer

NSCAT will be launched into a near-polar sun-synchronous orbit on the Japanese Advanced Earth Observing Satellite (ADEOS) in August 1996 on an H-II rocket from Tanegashima Space Center in Japan. The six antennas of NSCAT will send microwave pulses at a frequency of 14 GHz to the Earth's surface and measure the backscatter. The antennas will scan two 600-km bands of the ocean separated by a 330 km data gap. NSCAT measures the backscatter at 25 km resolution but will provide surface wind vector at 50 km resolution over 90% of the ice-free ocean every two days, under both clear and cloudy conditions. It will have considerably more than twice the coverage of the scatterometer on ERS 1 which scans only one 475 km band.

Standard data products will be distributed the Physical Oceanography Data Active Archive Center (PODAAC) of the Earth Observing System (EOS) at the Jet Propulsion Laboratory (JPL). The standard products include Levels 1.7,2, and 3. Level1.7 is earth-located normalized backscatter observed over ocean with quality flags, in wind vector cell in the ground tracks organized by NSCAT revolution. Level 2 includes multiple ocean wind vector solutions in wind vector cells with the selected wind vector flagged. Level 3 products are time and space averaged daily maps of wind vectors over global ocean on a 05° latitude by 0.5 longitude grid. A near real time fast data product will also be produced by the National Oceanic and Atmospheric Administration (NOAA) and will be available from NOAA and JPL. However, the fast product lacks the appropriate quality controls and error flags and the NSCAT Project is not responsible for its scientific integrity.

8. Sensor Synergism

With the planned launch of an improved scatterometer, SeaWinds, on ADEOS-2 in 1999, the acquisition of continuous data on ocean surface wind vectors for a period long enough to study the seasonal to interannual variability is being realized. It also signifies the continuous cooperation between Japan and the U.S.A. in providing long term ocean-wind and complementary data for monitoring, understanding, and predicting global climate and environmental changes. The scatterometer is the only spaceborne sensor that could provide direct (wind) and derived (current) dynamic measurements to study transport processes in the energy-hydrologic and biogeochemical cycles. Thus, it is complementary to other spaceborne sensors which measure hydrologic parameters, e.g., the operational Special Sensor Microwave Imager (SSMI) on the Defense Meteorological Space Program, the Advanced Microwave Scanning Radiometer (AMSR) to be launched in ADEOS-2, and suite of rain sensors on the joint U.S.-Japanese Tropical Rain Measuring Mission (TRMM). It is also complementary to sensors which measure ocean biological productivity, e.g., Ocean Color and Temperature Sensor (OCTS) to be launched with NSCAT on ADEOS-1 and the Global Imager (GLI) and ADEOS-2. The continuous acquisition of ocean surface wind vectors with complementary spacebased data, beyond ADEOS-2, satisfying the accuracy and sampling requirements equal or superior to the requirements for SeaWinds, is highly desirable to assure sufficient observations in the understanding of interannual variations and is crucial to the study of decadal global changes.

Acknowledgments

This study is performed at the Jet Propulsion Laboratory, California Institute of Technology, under contract with the National Aeronautics and Space Administration (NASA). It is support by the Topex/Poseidon, NASA Scatterometer (NSCAT), and Earth Observing System (EOS) Projects. We would like to thank Peter Niiler for providing the drifter data and Kelley Case for her assistant in processing these data.

References

Brown, R. A., and W.T. Liu, 1982: An operational large-scale marine boundary layer model. *J. Appl. Meteor., 21, 261-269.*

Brown, R. A., and G. Levy, 1986: Ocean surface pressure fields from satellite sensed winds. *Mon. Wea. Rev., 114, 2197-2206.*

Donelan, M. A., and W.J. Pierson, Jr., 1987: Radar scattering and equilibrium ranges in wind-generated waves with application to scatterometry. *J. Geophys. Res., 92, 4971-*5029.

Freilich, M.H., and R.S. Dunbar, 1993: A preliminary C-band scatterometer model function for the ERS- 1 AMI instrument. *Proc. First ERS-1 Symposium, ESA Sp-359, 79-84.*

Fu, L.L., W.T. Liu, and M. Abbott, 1990: Remote satellite method. *The Sea, Volume 9, Ocean Engineering Method.* JB. LeMehaute and D.M. Hanes (eds.) John Wiley & Sons, New York, 1193-1236

Hsu, C.S. and W.T. Liu, 1996: Surface wind and pressure field near tropical cyclone Oliver derived from ERS-1scatterometer observation, *J. Geophys. Res.,* submitted.

Glazman, R. E., G.G. Pihos, and J. Ip, 1988: Scatterometer wind-speed bias induced by the large-scale component of the wave field. *J. Geophys. Res.,* 9.?, 1317-1328.

Gyakum, J.R., 1983: On the evolution of the QE-II storm. 1: synoptic aspects. *Mon. Wea. Rev., 111,* 1137-1155$_0$

Krishnamurti, T.N., 1985: Summer monsoon experiment - a review. Mon. *Wea. Rev., 113,* 1590-1626.

Lau, K. M., and M.T. Li, 1984: The monsoon of east Asia and its global association - a survey. *Bull. Amer. Meteor. Sot., 65, 114-125.*

Liu, K.K, G.C. Gong, C.Z. Shyu, S.C. Psi, C.L. Wei, and S.Y. Chao, 1992: Response of Kuroshio upwelling to the onset of the northeast monsoon in the sea north of Taiwan: observations and a numerical simulation, *J. Geophys. Res.,* 97, 12511-12526,

Liu, W.T., K.B. Katsaros, and J.A. Businger, 1979: Bulk parametrization of air-sea exchanges of heat and water vapor including the **molecular** constraints at the interface. *J. Atmos. Sci.,* 36, 1722.-1735.

Liu, W. T., and W.G. Large, 1981: Determination of surface stress by Seasat-SASS; a case study with JASIN data, *J. Phys. Oceanogr., 11, 1603-1611.*

Liu, W.T., 1984: The effects of the variations in sea surface temperature and atmospheric stability in the estimation of average. wind speed by Seasat-SASS. *J. Phys. Oceanogr., 14, 392-401.*

Long, D.G., and J.M. Mendel, 1991: Identifiability in wind estimation from scatterometer measurements. *IEEE Trans. Geosci. Remote Sensing. 29, 268-276.*

Lukas, R., S. Hayes, and K. Wyrtki, Equatorial sea level response during the 1982-1983 El Nine, *J. Geophys. Res.,* 89, 10425, 1984

Luther, D. S., D. E. Harrison, and R. A. Knox, Zonal winds in the central equatorial Pacific, Science, 222,327,1983.

Rasmussen, E, M. and T. H. Carpenter, 1982: Variations in tropical sea surface temperature and surface wind fields associated with the Southern *Oscillation* El *Nine, Mon. Wea. Rev. 110,* 354.

Niiler, P., A. S." Sybrandy, K. Bi, P.M. Poulain, and D. Bitterman: Measurements of water following capability of holey sock and TRISTAR drifters. *Deep-Sea Res.,* 42, 1951-1964.

Plant, W. J., 1986: A two-scale model of short wind-generated waves and scatterometry. *J. Geophys. Res., 91,* 10735-10749.

Ralph, E. A., and P. Niiler, 1995: Lagrangian measurement of the mean wind-driven currents in the tropical Pacific. *International WOCE Newsletter, 30.*

Ramage, C. S., 1971: *Monsoon Meteorology.* Academic Press, New York, 296 pp.
Stewart, R.H., 1985: *Methods of Satellite Oceanography.* Univ. of Calif. Press. San Diego, Ca, 360pp.
Weissman, D.E.. ILL. Davidson, R.A. Brown, C.A. Friehe, and F. Li, 1994: The relationships betwen microwave radar corss section and both wind speed and stress: model function studies using Frontal Air-sea Interaction Experiment data. *J. Geophys. Ii'cS.,* 99, 10087-10108.
Wentz, F. J., S. Peteherych, and L.A. Thomas, 1984: A model function for ocean radar cross sections at 14.6 Ghz. *J. Geophys. Res., 89, 3689-3704.*